

Development of a Prediction System for 3D Printed Part Deformation

Hong-Seok Park

School of Mechanical and Automotive Engineering
University of Ulsan
Ulsan, Republic of Korea
phosk@ulsan.ac.kr

Ngoc-Hien Tran

Faculty of Mechanical Engineering
University of Transport and Communications
Hanoi, Vietnam
tranhien.tkm@utc.edu.vn

Van-Thong Hoang

Faculty of Information Technology
University of Transport and Communications
Hanoi, Vietnam
thonghv@utc.edu.vn

Vu-Hung Bui

Faculty of Mechanical Engineering
University of Transport and Communications
Hanoi, Vietnam
bvhung.tkm@utc.edu.vn

Received: 12 August 2022 | Revised: 26 August 2022 | Accepted: 2 September 2022

Abstract-The Additive Manufacturing (AM) process is applied in industrial applications. However, quality issues of the printed parts, including part distortion and cracks caused by high temperature and fast cooling, result in high residual stress. The theoretical calculation equation shows elastic behavior which is the linear behavior between strain and stress. However, in practice with the additive manufacturing process, strain and stress have nonlinear behavior. So, the prediction of the deformation of a printed part is inaccurate. The contribution of this research is the creation of an Inherent Strain (IS)-based part deformation prediction method during the Selective Laser Melting (SLM) process. To have the deformation in the design stage, we developed software for calculating the IS value and predicting the deformation. The difference between the calculated results and the experimental results is still there, so, we proposed an algorithm and developed an optimization module for the system to minimize this difference. In the final optimal printing process, the parameters are derived in order for the real printing process to have the required quality of the SLM printed part.

Keywords-selective laser melting; predicting deformation; inherent strain; heat treatment effect zone

I. INTRODUCTION

Layer by layer manufacturing or additive manufacturing has been used in many application fields such as aerospace, automotive, biomedical, and energy production and distribution. The printed parts are made from plastic or metal powder materials [1-4]. However, the quality issues of the printed parts, including part distortion, as well as the cracks caused by high temperature and fast cooling, result in high residual stress. This is a challenge that limits the industry acceptance of AM. To overcome this challenge, a numerical modeling method for predicting the part distortion at the design stage plays an important role, which enables design engineers

to remove failures before carrying out printing as well as to determine the optimal printing process parameters to minimize part deformation. Currently, with the rapid growth of this technology, many AM processes have been applied in industrial applications. Selective Laser Melting (SLM) is one of these AM processes. SLM is an AM process that directly produces parts from metal powder. SLM is a complex thermal-physical-chemical process of the interaction between a laser source and metallic powders [1, 5]. The SLM mechanism is shown in Figure 1. The SLM system includes the laser source, the optical system, and the deposition system. The optical system has the optical mirrors which enable the laser source to be directed onto the powder bed surface. The thin powder layer is distributed by the deposition system and melted by the laser source through the optical system. The deposition system that is the scraper or roller system enables the distribution of the powder onto the printed area. The printed layer thickness is determined by the distance of moving down of the build platform. Then, another powder layer is added on the top of the printed previous layer. This step is repeated until the entire 3D model is completed.

For printing the metal parts, there are currently many different AM processes using different combinations of stock material form, material delivery, and heat source. SLM is the most attractive method for layer by layer building of metal parts due to advantages such as the lack of post-processing. However, as the same with other AM processes, the distortion and cracks of the printed parts still occur due to the residual stress caused by the rapid heating and cooling process [6]. In the SLM process, high temperature is required for the melting of the metallic powders. Due to high temperature and fast cooling, residual stress will be generated in the printed part. The large residual stress results in part distortion which is a negative effect of the product performance. Part distortion caused by the tensile residual stress not only reduces the part

geometrical accuracy, but also affects the functional performance of the printed parts. To acquire good printed part quality, key factors such as powder properties, printing process parameters, and SLM machine characteristics must be considered.

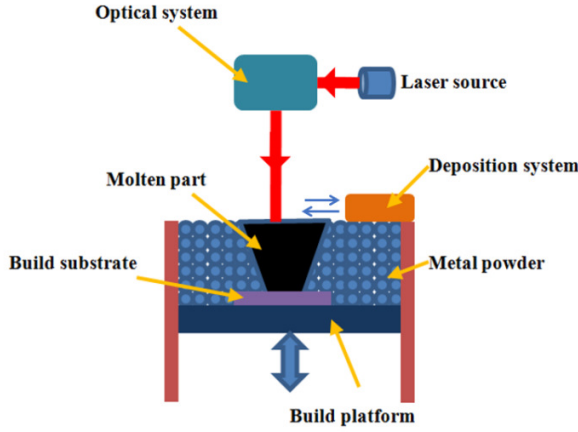


Fig. 1. Mechanism of the selective laser melting process.

Currently, the method for keeping the quality of the printed part is trial-and-error testing. This method depends on the user's experience and requires larger manufacturing costs, while producing waste and scrap [7]. Therefore, it is necessary for predicting the part's quality at the design stage which enables to remove failures before carrying out the real printing. Many researchers have used the inherent strain method for predicting part deformation in welding processes. However, some proposals for modifying the conventional IS method have been applied to apply this method to AM processes such as the SLM process, [8, 9]. Authors in [9] proposed the extraction of the IS value from micro-scale thermo-mechanical analysis. This IS value was applied to the part-scale model to have the part deformation. However, it is challenging to predict the residual deformation in the part-scale model [10]. To overcome this challenge, a multi-scale modeling approach is proposed in [11, 12]. Currently, some commercial tools based on the IS method enable the prediction of deformation. However, the algorithms to calculate the IS value and how to apply this value to the part-scale model are not publicly available [13].

This paper presents a new method for predicting the deformation of the 3D printed part using the ISs. For carrying out this research, a method for calculating the IS value is proposed. These IS values are used for calculating the deformation. Both simulation and experiments were implemented for comparing the IS values and deformations.

II. MODEL FOR DETERMINING THE IS VALUE

A. Theoretical Model

The term of IS was firstly introduced in 1975 for analyzing the welding process. It is a general name for the expression of non-elastic strains which include the thermal strain $\epsilon_{thermal}$, phase transfer strain ϵ_{phase} , plastic strain $\epsilon_{plastic}$, and creep strain ϵ_{creep} [7]. During the SLM process with the heating and

cooling cycles, the total strain is the sum of the elastic strain $\epsilon_{elastic}$ and IS ϵ^* , as shown below:

$$\epsilon_{total} = \epsilon_{elastic} + \epsilon^* \quad (1)$$

The inherent strain is calculated as:

$$\epsilon^* = \epsilon_{thermal} + \epsilon_{plastic} + \epsilon_{phase} + \epsilon_{creep} \quad (2)$$

Strain and stress are unknown variables. We can determine the value of one of these variables by experiments. The remaining variable is determined by the equation showing the relationship between strain and stress. The commercial tools enable engineers to estimate the IS value. However, the algorithms for calculating the IS value are not published. During the printing process, the material begins at the melting temperature via the heating stage and is changed to a lower temperature via the cooling stage at a high rate. The material of the printed part will receive a compressive force due to the thermal change. Thus, the three-dimensional ISs are compressive strains, and the equations can be defined as [14]:

$$\epsilon_x^* = -\frac{W_x}{F_x}; \epsilon_y^* = -\frac{W_y}{F_y}; \epsilon_z^* = -\frac{W_z}{F_z} \quad (3)$$

in which F_x , F_y , and F_z are the zone areas where W_x , W_y , and W_z respectively are distributed. The total volume W_x of ϵ_x^* , the total volume W_y of ϵ_y^* , and the total volume W_z of ϵ_z^* in unit length are calculated as follows:

$$W_x = \zeta \cdot q_v; W_y = W_z = K \cdot q_v \quad (4)$$

in which q_v is the linear energy density (J/mm) [15]:

$$q_v = \frac{Q_{heat\ source}}{u} \quad (5)$$

ζ and K (mm/J) are longitudinal and transverse inherent strain coefficients, respectively. Figure 2 shows the components of the inherent strain ϵ_x , ϵ_y , and ϵ_z with these parameters.

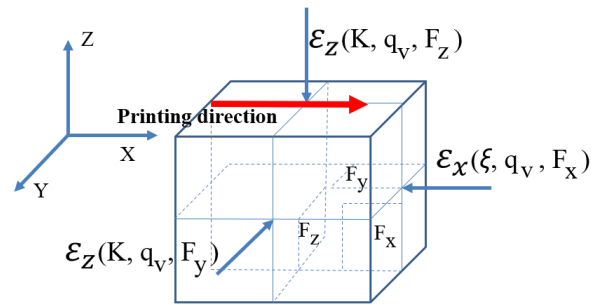


Fig. 2. Inherent strain components.

The inherent strains in the x, y, and z directions for the first layer are calculated as follows:

$$\epsilon_{inh-x} = -\frac{\xi \cdot q_v}{F_x}; \epsilon_{inh-y} = -\frac{K \cdot q_v}{F_y}; \epsilon_{inh-z} = -\frac{K \cdot q_v}{F_z} \quad (6)$$

Figure 3 shows the calculation of the IS for n layers. After printing the first layer, the IS value is ϵ_{inh} . If we add the second layer via the SLM process mechanism, the first layer is re-melted with the new heat treatment effect zone, so the remaining IS value for the first layer is:

$$\varepsilon'_1 = \varepsilon_{inh} - \frac{d}{h} \varepsilon_{inh} \quad (7)$$

When the second layer is added, its IS value is:

$$\varepsilon_2 = \varepsilon'_1 + \varepsilon_{inh} = 2\varepsilon_{inh} - \frac{d}{h} \varepsilon_{inh} \quad (8)$$

If a third layer is added, the remaining IS value in the second layer is:

$$\varepsilon'_2 = \varepsilon_2 - \frac{d}{h} \varepsilon_{inh} = 2\varepsilon_{inh} - \frac{2d}{h} \varepsilon_{inh} \quad (9)$$

and the IS value in the third layer is calculated as:

$$\varepsilon_3 = \varepsilon'_2 + \varepsilon_{inh} = 3\varepsilon_{inh} - \frac{2d}{h} \varepsilon_{inh} \quad (10)$$

Repeating this SLM process for n layers, we can calculate the IS value for the n^{th} layer as follows:

$$\varepsilon_n = \varepsilon'_{n-1} + \varepsilon_{inh} = n\varepsilon_{inh} - \frac{(n-1)d}{h} \varepsilon_{inh} \quad (11)$$

For whole part, in x , y , and z directions, we have the IS value as follows:

$$\begin{cases} \varepsilon_x (n \text{ layer}) = n\varepsilon_{inh-x} - \frac{(n-1)d}{h} \varepsilon_{inh-x} \\ \varepsilon_y (n \text{ layer}) = n\varepsilon_{inh-y} - \frac{(n-1)d}{h} \varepsilon_{inh-y} \\ \varepsilon_z (n \text{ layer}) = n\varepsilon_{inh-z} - \frac{(n-1)d}{h} \varepsilon_{inh-z} \end{cases} \quad (12)$$

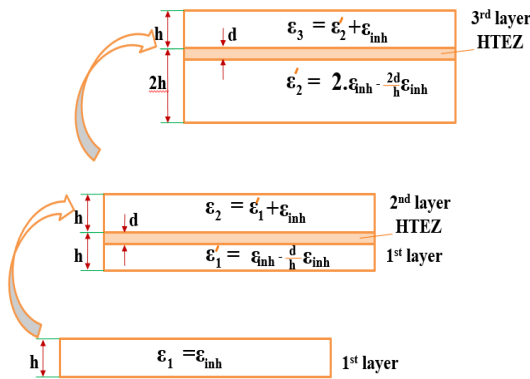


Fig. 3. Method for calculating inherent strain for whole part.

B. Simulation and Experiments

1) Simulation Results

The mathematical model of the heat transfer, which we used to determine the temperature distribution during the SLM process, is [16]:

$$\rho C \frac{\partial T}{\partial t} + \rho C u \nabla T = \nabla(k \nabla T) + Q_G \quad (13)$$

where T is the temperature, ρ , C , and k are density, thermal capacity, and thermal conductivity factor respectively, u is the printing speed. Q_G is the power distribution given by the moving Goldak's double-ellipsoid heat source model as shown in Figure 4 [17], this heat source model from the welding process, however, it is also suitable for research on the SLM process. Q_G is the total of the absorbed laser in front and rear

of the Goldak heat source model [18]. We used this heat transfer model and printing process parameters (as shown in Table I) for simulation using ComsolTM. We also run tests with the same material (316L steel), however, with differences in the printing process parameters (300W laser power, 1300mm/s laser velocity, and 0.045mm layer thickness). In this case, the inherent strain in Z direction is -0.153 [19].

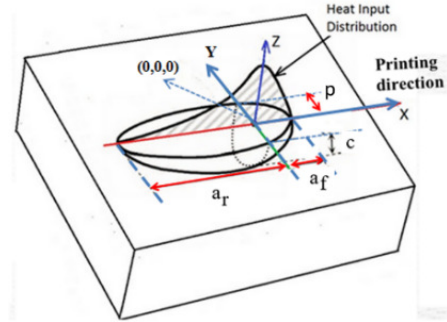


Fig. 4. Goldak heat source in the finite element model of the AM process.

The temperature distribution during the SLM process is shown in Figure 5. The Heat Treatment Effect Zone (HTEZ) surfaces are shown in Figures 6-8. The HTEZ surface in the ZX plane as shown in Figure 6 is calculated as follows:

$$F_x = (x + e) \cdot d - e \cdot c \quad (14)$$

with $d = 0.112\text{mm}$, $c = 0.0522\text{mm}$, $e = 0.5255\text{mm}$, and $x = 2.429\text{mm}$, we have $F_x = 0.3035\text{mm}^2$.

The HTEZ surface in the XY plane as shown in Figure 7 is calculated as follows:

$$F_y = 2(x + e) \cdot (a + b) - 2a \cdot e - f \cdot n \quad (15)$$

with $a = 0.089\text{mm}$, $b = 0.137\text{mm}$, $e = 0.5255\text{mm}$, $f = 0.258$, $n = 3.166$, and $x = 2.429\text{mm}$, we have $F_y = 0.425\text{mm}^2$.

The HTEZ surface in the ZY plane as shown in Figure 8 is calculated as:

$$F_z = 2[(a + b) \cdot d - a \cdot c] \quad (16)$$

with $a = 0.089\text{mm}$, $b = 0.137\text{mm}$, $d = 0.112\text{mm}$, and $c = 0.0522\text{mm}$, we have $F_z = 0.0413\text{mm}^2$.

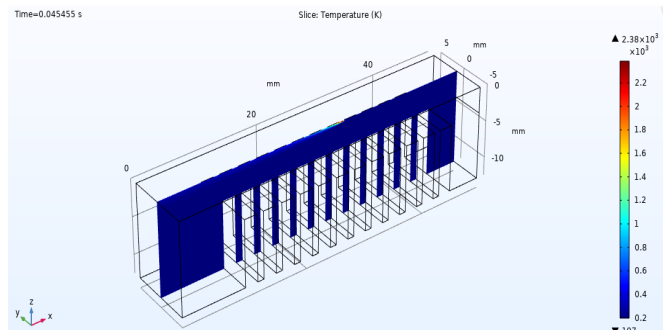


Fig. 5. Goldak heat source in the finite element model of the AM process.

TABLE I. PRINTING PROCESS PARAMETERS [18]

Name	Description	Value
x_0	Path center X-Coordinate	0mm
y_0	Path center Y-Coordinate	0mm
$Q_{heat\ source}$	Laser power	250W
p	Length of the y-semi-axis of ellipsoid (mm)	0.173mm
c	Length of the z-semi-axis of ellipsoid (mm)	0.230mm
a_f	Length of the x-semi-axis of front ellipsoids (mm)	0.173mm
a_r	Length of the x-semi-axis of rear ellipsoids (mm)	0.347mm
u	Laser velocity	1100mm/s
C	Thermal capacity	$500 \times 10^{-3} \text{J}/(\text{g.K})$
λ	Thermal conductivity factor	$19.4 \times 10^{-3} \text{W}/(\text{mm.K})$
T_a	Ambient temperature	293K
h	Layer thickness	0.05mm
ha	Hatch distance	0.07mm

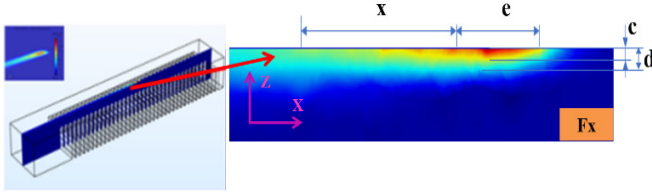


Fig. 6. HTEZ surface in in the ZX plane.

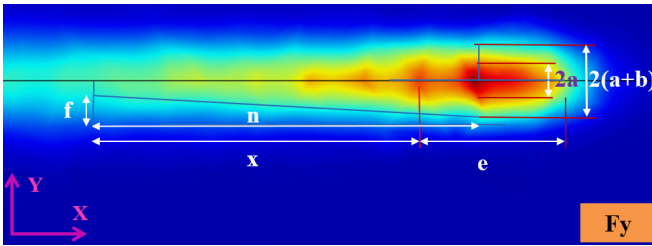


Fig. 7. HTEZ surface in in the XY plane.

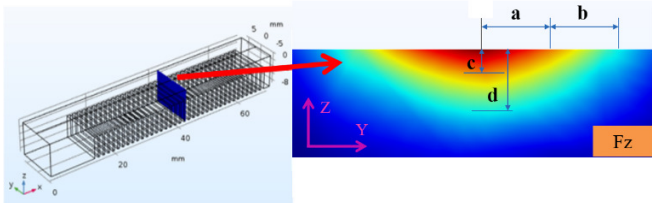


Fig. 8. HTEZ surface in in the ZY plane.

The inherent strains in the x , y , and z directions for the first layer are calculated by applying (6) with $\zeta = 1.57 \times 10^{-3} \text{mm}^3/\text{J}$, $K = 0.58 \times 10^{-3} \text{mm}^3/\text{J}$ [14], and $q_v = 0.2273 \text{J}/\text{mm}$ for 316L stainless steel, $F_x = 0.3035 \text{mm}^2$, $F_y = 0.425 \text{mm}^2$, and $F_z = 0.0413 \text{mm}^2$, we have: $\epsilon_{inh-x} = -0.00118$, $\epsilon_{inh-y} = -0.00031$ and $\epsilon_{inh-z} = -0.003$. In comparison with the reported IS value for the first layer in the welding process, which also considers the influence of the temperature distribution to the IS value, the calculated IS value is acceptable. In the z direction, where the highest temperature is 1500°C (or 1773°K) the inherent strain value is 0.0017 [20]. Thus, the IS value for the whole part after 60 printed layers

(with layer thickness of 0.05mm and printed part height of 3mm) is calculated as follows: Assuming that the depth (d) that affects the inherent strain distribution equals to $(1/3)$ of the layer thickness (h), we have the following IS values using (12): $\epsilon_x(\text{whole part}) = -0.04742$, $\epsilon_y(\text{whole part}) = -0.0125$, $\epsilon_z(\text{whole part}) = -0.1286$.

2) Experimental Results

Experiments on printing a cantilever beam were carried out on an SLM machine at the Laboratory of Production Engineering, Ulsan University, Republic of Korea (Figure 9). The geometrical model of the cantilever beam and the printing direction (0° , 45° , and 90°) are shown in Figure 10. Specimens were printed on the MetalSys 250.

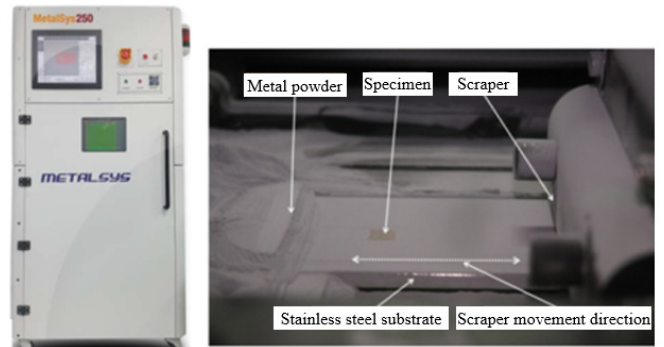


Fig. 9. Experiments on the SLM machine.

The highest deformation of the cantilever beam at the position in the z direction with 0° printing direction after cutting the part from the base plate by the Electrical Discharge Machining (EDM) machine is 1.45mm as shown in Figure 9 and Table II. The IS is calculated as follows:

$$\epsilon = -\frac{l_t - l_0}{l_0} = -\frac{13.95 - 12.5}{12.5} = -0.116 \quad (17)$$

where l_0 is the part length before cutting by EDM and l_t is the part length after cutting by EDM. Considering the z direction, with the part height before and after cutting being 12.5mm and 13.95mm, we have $\epsilon_z = -0.116$, and the deformation in the z direction is 1.45mm. The IS value in the z direction predicted by simulation is -0.1286 . The difference between simulation and experiment is considered acceptable.

TABLE II. GEOMETRY MEASUREMENT AFTER CUTTING

Geometry measurement	Distortion (mm)					
	1	2	3	4	5	Average
Scan pattern (0°)	13.93	13.94	13.96	14.02	13.90	13.95
Scan pattern (90°)	13.24	13.19	13.21	13.19	13.12	13.19
Scan pattern (45°)	13.50	13.48	13.50	13.51	13.43	13.484

With the proposed method, the IS value in the z direction is $\epsilon_z = -0.1286$. From this IS value, with a total part height of $H = 12.5 \text{mm}$, the deformation (δ) of the printed part in the Z direction is 1.608mm, which is calculated by:

$$\delta = |\epsilon_z(\text{whole part})| \cdot H \quad (18)$$



Fig. 10. Specimens printed by SLM.

III. ARCHITECTURE OF FUNCTIONALITY MODULES

A. Module for Calculating the HTEZ Surfaces

To develop the proposed system, we drive out the architecture of functionality modules. Figure 11 shows the architecture of the module for calculating HTEZ surfaces. With the input parameters such as 3D model of part, layer thickness (h), hatch distance (ha), scanning speed (u), and laser power (Q), the databases of the system are updated which are printing parameter database and part dimension database. In the printing parameter database u , Q and the heat source (Goldak model) with parameters such as c , b , a_f , a_r , are used for calculating the absorbed laser. Other databases are also built which are the material properties (thermal capacity, thermal expansion, and thermal conductivity factor), and the coefficient for printing (lattice parameter, laser interaction time). The thermal capacity (C) in material properties database and the absorbed laser are used for calculating the temperature distribution through the heat transfer equation. From the temperature distribution and the material properties and coefficient for printing databases, we have the HTEZ parameters (x , e , c , d , a , b , f , n). Then, we calculate the HTEZ surfaces (F_x , F_y , F_z).

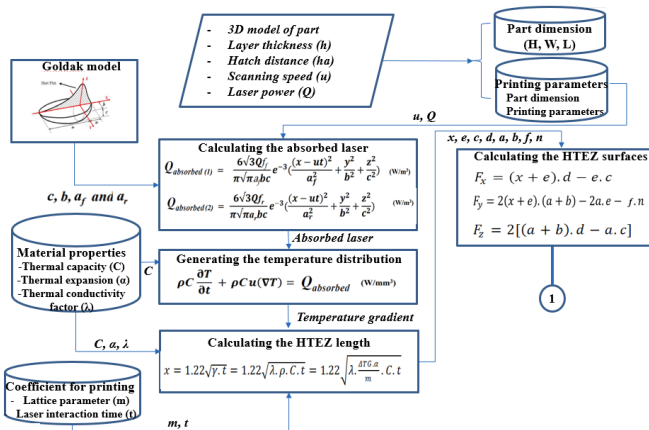


Fig. 11. Architecture of the module for calculating HTEZ surfaces.

B. Module for Calculating the IS for One Layer

Figure 12 shows the architecture of the module for calculating the IS value for one layer. With the input parameters including the printing process parameters, and the HTEZ surfaces, the system allows to calculate the melting energy, the laser power, and the linear energy density. Then, the linear energy density (q_v) and the layer thickness are used for calculating the longitudinal, transverse IS coefficients (ζ , K). From the q_v , ζ , and K , we calculate the IS value for one layer using (6).

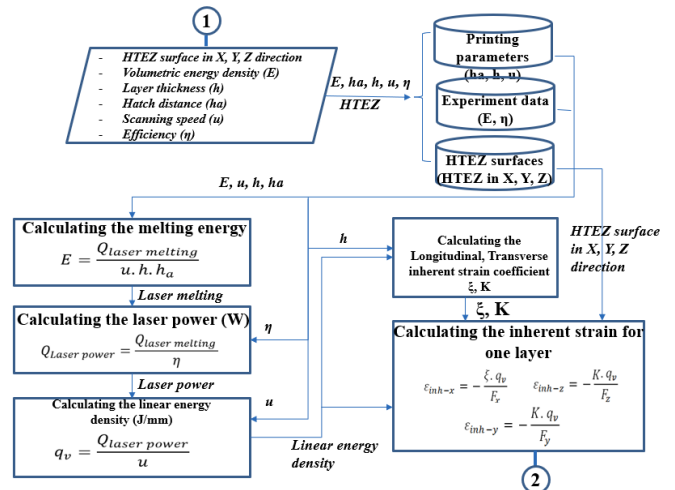


Fig. 12. Architecture of the module for calculating IS for one layer.

C. Module for Calculating the IS for the Whole Part

Figure 13 shows the architecture of the module for calculating the IS value for whole part. With the input parameters including the IS value for one layer, part dimension, and printing parameters, the layer number and the HTEZ depth are calculated. Then, these data are used for calculating the IS value for the whole part using (12).

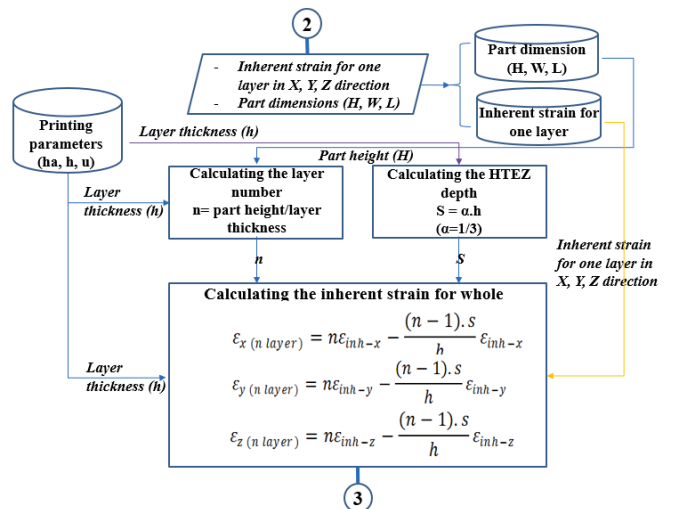


Fig. 13. Architecture of the module for calculating the IS for the whole part.

D. Module for Optimizing the Difference Between the Simulations and the Experiments

Figure 14 shows the architecture of the module for optimizing the difference between the simulations and the experiments. From the simulation and experimental results, the system enables to calculate the new IS value in case the difference between them in the printed part deformation is more than 0.01.

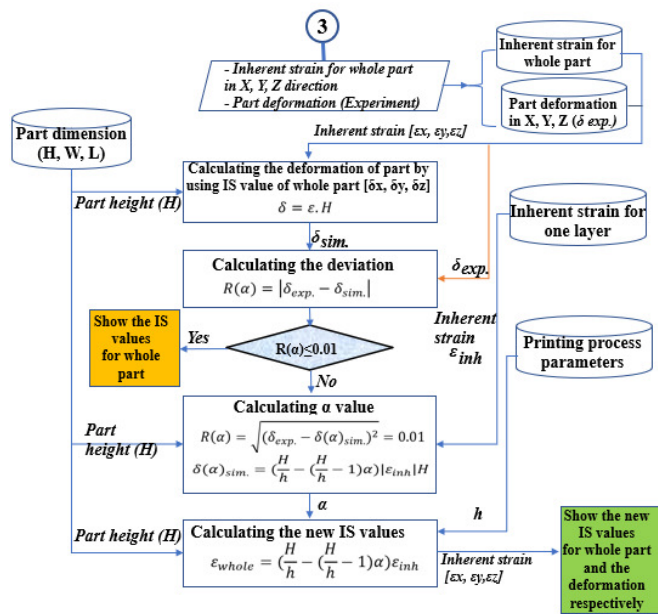


Fig. 14. Architecture of the module for optimizing the difference between the simulation and experiment.

IV. IMPLEMENTATION OF THE SYSTEM

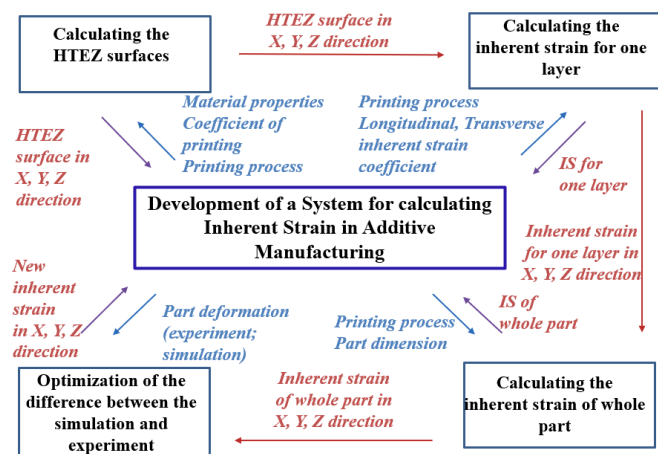


Fig. 15. Architecture of the system for calculating inherent strain.

To acquire the deformation in the design stage, we developed software for calculating the IS and for predicting the printed part deformation. The developed system includes 4 modules: a module for calculating the HTEZ surfaces, a module for calculating the IS for one layer, a module for

calculating the IS of whole part, and a module for optimizing the difference between the simulations and the experiments.

For programming the proposed system, we used C++ language in Visual Studio 2019 environment. The system architecture is shown in Figure 15 which describes the information flow among the modules. Figure 16 shows the interface module which shows the integration of modules for one complete system. With the input data including printing process parameters (such as volumetric energy density, layer thickness, hatch distance, scanning speed, and efficiency) and the HTEZ surfaces, the developed system allows to calculate the IS value for one layer as shown in Figure 17. The volumetric energy density value is 40J/mm³ [21]. From the calculated IS values for one layer and part information (such as length, width, and part height), the developed system enables to calculate the IS value of the whole part in x, y, z directions as shown in Figure 18.



Fig. 16. Screenshot of the system interface with four modules.

V. CONCLUSION

The contribution of this research is the creation of an inherent strain-based part deformation prediction method during the Selective Laser Melting (SLM) process. To determine the Inherent Strain (IS) value, a micro-scale model for analyzing the temperature distribution was created. The IS value for one layer is calculated from the temperature gradient. For calculating the IS value for the whole part, the HTEZ is used. Then, the IS value is used to determine the part deformation. The proposed methodology has been developed and evaluated using 316L stainless steel cantilever beams, and both simulated and experimental results were obtained. To acquire the deformation in the design stage, we developed the IS-based deformation prediction software. The functionality of the developed system was tested successfully.

Future research can be conducted with the consideration of other factors affecting the printed part quality in order to minimize part deformation. In addition, other printing processes also should be added to the developed system.

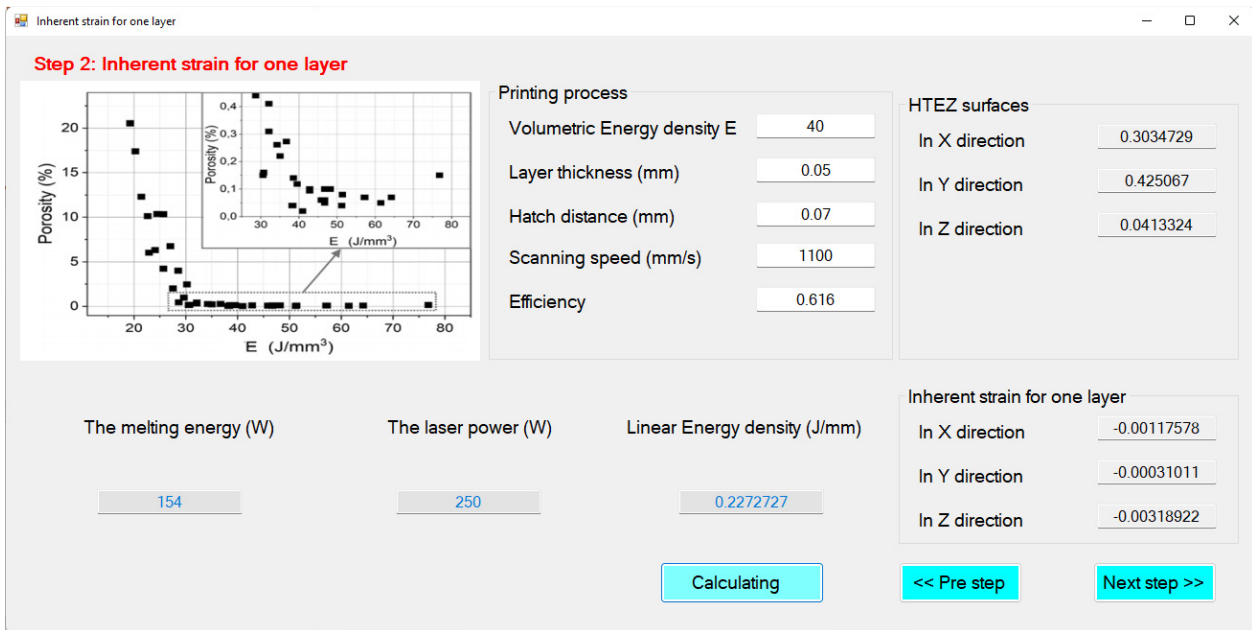


Fig. 17. Screenshot of the module for calculating inherent strain for one layer.

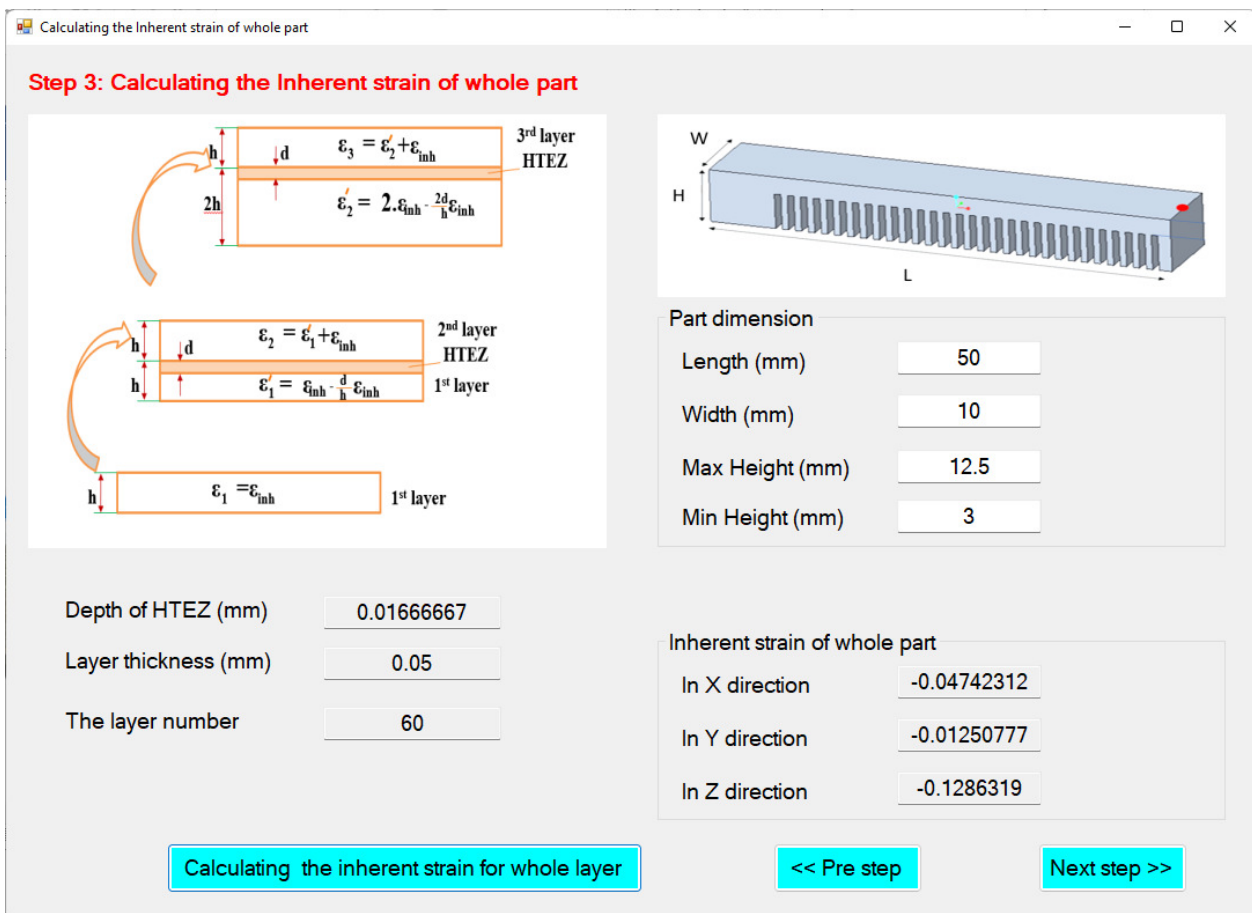


Fig. 18. Screenshot of the module for calculating IS of whole part.

ACKNOWLEDGMENT

This research is funded by the University of Transport and Communications (UTC) under grant number T2022-CK-12, supported by the University of Ulsan.

REFERENCES

- [1] T. Sunar and M. Cetin, "An Experimental Study on Boron Carbide Reinforced Open Cell Aluminum Foams Produced via Infiltration Technique," *Engineering, Technology & Applied Science Research*, vol. 8, no. 6, pp. 3640–3645, Dec. 2018, <https://doi.org/10.48084/etasr.2419>.
- [2] D. G. Zisopol, I. Nae, A. I. Portoaca, and I. Ramadan, "A Statistical Approach of the Flexural Strength of PLA and ABS 3D Printed Parts," *Engineering, Technology & Applied Science Research*, vol. 12, no. 2, pp. 8248–8252, Apr. 2022, <https://doi.org/10.48084/etasr.4739>.
- [3] D. G. Zisopol, I. Nae, A. I. Portoaca, and I. Ramadan, "A Theoretical and Experimental Research on the Influence of FDM Parameters on Tensile Strength and Hardness of Parts Made of Poly(lactic Acid)," *Engineering, Technology & Applied Science Research*, vol. 11, no. 4, pp. 7458–7463, Aug. 2021, <https://doi.org/10.48084/etasr.4311>.
- [4] D. G. Zisopol, A. I. Portoaca, I. Nae, and I. Ramadan, "A Comparative Analysis of the Mechanical Properties of Annealed PLA," *Engineering, Technology & Applied Science Research*, vol. 12, no. 4, pp. 8978–8981, Aug. 2022, <https://doi.org/10.48084/etasr.5123>.
- [5] B. Schoinochoritis, D. Chantzis, and K. Salonitis, "Simulation of metallic powder bed additive manufacturing processes with the finite element method: A critical review," *Proceedings of the Institution of Mechanical Engineers, Part B: Journal of Engineering Manufacture*, vol. 231, no. 1, pp. 96–117, Jan. 2017, <https://doi.org/10.1177/0954405414567522>.
- [6] E. Kundakcioglu, I. Lazoglu, and S. Rawal, "Transient thermal modeling of laser-based additive manufacturing for 3D freeform structures," *The International Journal of Advanced Manufacturing Technology*, vol. 85, no. 1, pp. 493–501, Jul. 2016, <https://doi.org/10.1007/s00170-015-7932-2>.
- [7] I. Setien, M. Chiumenti, S. van der Veen, M. San Sebastian, F. Garcandiá, and A. Echeverría, "Empirical methodology to determine inherent strains in additive manufacturing," *Computers & Mathematics with Applications*, vol. 78, no. 7, pp. 2282–2295, Oct. 2019, <https://doi.org/10.1016/j.camwa.2018.05.015>.
- [8] M. Bugatti and Q. Semeraro, "Limitations of the inherent strain method in simulating powder bed fusion processes," *Additive Manufacturing*, vol. 23, pp. 329–346, Oct. 2018, <https://doi.org/10.1016/j.addma.2018.05.041>.
- [9] X. Liang, Q. Chen, L. Cheng, Q. Yang, and A. To, "A Modified Inherent Strain Method for Fast Prediction of Residual Deformation in Additive Manufacturing of Metal Parts," in *Solid Freeform Fabrication 2017: Proceedings of the 28th Annual International Solid Freeform Fabrication Symposium – An Additive Manufacturing Conference*, Austin TX, USA, 2017, <https://doi.org/10.26153/tsw/16972>.
- [10] X. Liang, Q. Chen, L. Cheng, D. Hayduke, and A. C. To, "Modified inherent strain method for efficient prediction of residual deformation in direct metal laser sintered components," *Computational Mechanics*, vol. 64, no. 6, pp. 1719–1733, Dec. 2019, <https://doi.org/10.1007/s00466-019-01748-6>.
- [11] S. N. Ahmad *et al.*, "FEM Simulation Procedure for Distortion and Residual Stress Analysis of Wire Arc Additive Manufacturing," *IOP Conference Series: Materials Science and Engineering*, vol. 834, no. 1, Dec. 2020, Art. no. 012083, <https://doi.org/10.1088/1757-899X/834/1/012083>.
- [12] M. Schänzel, A. Ilin, and V. Ploshikhin, "New approach for fast numerical prediction of residual stress and distortion of AM parts from steels with phase transformations," in *10th International Seminar 'Numerical Analysis of Weldability*, Gratz, Austria, Sep. 2012, <https://doi.org/10.3217/978-3-85125-615-4-54>.
- [13] Q. Chen *et al.*, "An inherent strain based multiscale modeling framework for simulating part-scale residual deformation for direct metal laser sintering," *Additive Manufacturing*, vol. 28, pp. 406–418, Aug. 2019, <https://doi.org/10.1016/j.addma.2019.05.021>.
- [14] L. Yazhi, "Research on Inherent Strain Distribution in Welded Low-Alloy Components," in *2014 Sixth International Conference on Measuring Technology and Mechatronics Automation*, Jan. 2014, pp. 512–515, <https://doi.org/10.1109/ICMTMA.2014.125>.
- [15] Č. Donik, J. Kraner, I. Paulin, and M. Godec, "Influence of the Energy Density for Selective Laser Melting on the Microstructure and Mechanical Properties of Stainless Steel," *Metals*, vol. 10, no. 7, Jul. 2020, Art. no. 919, <https://doi.org/10.3390/met10070919>.
- [16] A. A. Saprykin, E. A. Ibragimov, and E. V. Babakova, "Modeling the Temperature Fields of Copper Powder Melting in the Process of Selective Laser Melting," *IOP Conference Series: Materials Science and Engineering*, vol. 142, Dec. 2016, Art. no. 012061, <https://doi.org/10.1088/1757-899X/142/1/012061>.
- [17] Z. Samad, N. M. Nor, and E. R. I. Fauzi, "Thermo-Mechanical Simulation of Temperature Distribution and Prediction of Heat-Affected Zone Size in MIG Welding Process on Aluminium Alloy EN AW 6082-T6," *IOP Conference Series: Materials Science and Engineering*, vol. 530, no. 1, Mar. 2019, Art. no. 012016, <https://doi.org/10.1088/1757-899X/530/1/012016>.
- [18] V. Nain, T. Engel, M. Carin, D. Boisselier, and L. Seguy, "Development of an Elongated Ellipsoid Heat Source Model to Reduce Computation Time for Directed Energy Deposition Process," *Frontiers in Materials*, vol. 8, 2021, <https://doi.org/10.3389/fmats.2021.747389>.
- [19] H.-S. Park, H. S. Shin, and N.-H. Tran, "A new approach for calculating inherent strain and distortion in additive manufacturing of metal parts," *The International Journal of Advanced Manufacturing Technology*, vol. 121, no. 9, pp. 6507–6521, Aug. 2022, <https://doi.org/10.1007/s00170-022-09766-0>.
- [20] T.-J. Kim, B.-S. Jang, and S.-W. Kang, "Welding deformation analysis based on improved equivalent strain method considering the effect of temperature gradients," *International Journal of Naval Architecture and Ocean Engineering*, vol. 7, no. 1, pp. 157–173, Jan. 2015, <https://doi.org/10.1515/ijnaoe-2015-0012>.
- [21] A. Leicht, M. Fischer, U. Klement, L. Nyborg, and E. Hryha, "Increasing the Productivity of Laser Powder Bed Fusion for Stainless Steel 316L through Increased Layer Thickness," *Journal of Materials Engineering and Performance*, vol. 30, no. 1, pp. 575–584, Jan. 2021, <https://doi.org/10.1007/s11665-020-05334-3>.